Available online at www.sciencedirect.com

SCIENCE DIRECT

Virology 339 (2005) 56 – 69

VIROLOGY

www.elsevier.com/locate/yviro

Scrambling of the amino acids within the transmembrane domain of Vpu results in a simian-human immunodeficiency virus ($SHIV_{TM}$) that is less pathogenic for pig-tailed macaques

David R. Hout[a], Melissa L. Gomez[a], Erik Pacyniak[a], Lisa M. Gomez[a], Sarah H. Inbody[a], Ellyn R. Mulcahy[a], Nathan Culley[b], David M. Pinson[c], Michael F. Powers[d], Scott W. Wong[d], Edward B. Stephens[a,*]

[a]*Department of Anatomy and Cell Biology, University of Kansas Medical Center, 3901 Rainbow Boulevard, Kansas City, KS 66160, USA*
[b]*Laboratory Animal Resources, University of Kansas Medical Center, 3901 Rainbow Boulevard, Kansas City, KS 66160, USA*
[c]*Department of Laboratory Medicine and Pathology, University of Kansas Medical Center, 3901 Rainbow Boulevard, Kansas City, KS 66160, USA*
[d]*Vaccine and Gene Therapy Institute, Oregon Health Sciences University, Beaverton, OR 97003, USA*

Received 20 January 2005; returned to author for revision 3 March 2005; accepted 12 April 2005
Available online 21 June 2005

Abstract

Previous studies have shown that the transmembrane (TM) domain of the subtype B Vpu enhances virion release from cells and some studies have shown that this domain may form an oligomeric structure with properties of an ion channel. To date, no studies have been performed to assess the role of this domain in virus pathogenesis in a macaque model of disease. Using a pathogenic molecular clone of simian human immunodeficiency virus ($SHIV_{KU\text{-}1bMC33}$), we have generated a novel virus in which the transmembrane domain of the Vpu protein was scrambled but maintained hydrophobic in nature ($SHIV_{TM}$), which presumably would disrupt any ion channel TM properties of this protein. Vectors expressing the Vpu as a fusion protein with the enhanced green fluorescent protein ($Vpu_{TM}EGFP$) indicate that it was transported to the same intracellular compartment as the unmodified Vpu protein but did not down-regulate cell surface expression of CD4. To assess the pathogenicity of $SHIV_{TM}$, three pig-tailed macaques were inoculated with the $SHIV_{TM}$ and monitored for 6–8 months for $CD4^+$ T cell levels, viral loads and the stability of the sequence of the *vpu* gene. Our results indicated that unlike the parental $SHIV_{KU\text{-}1bMC33}$, inoculation of macaques with $SHIV_{TM}$ did not cause a severe $CD4^+$ T cell loss over the course of their infections. Sequence analysis of the *vpu* gene analyzed from sequential PBMC samples derived from macaques revealed that the scrambled TM was stable during the course of infection. At necropsy, examination of tissues revealed low viral loads and none of the pathology commonly observed in lymphoid and non-lymphoid tissues following inoculation with the pathogenic parental $SHIV_{KU\text{-}1bMC33}$ virus. Thus, these results show for the first time that the TM domain of Vpu contributes to the pathogenicity of $SHIV_{KU\text{-}1bMC33}$ in pig-tailed macaques.

Keywords: Vpu; Transmembrane domain; Pathogenesis; SHIV; HIV-1

Introduction

The Vpu protein is the smallest membrane protein encoded by human immunodeficiency virus type 1 (HIV-1), which consists of a short amino terminal domain, an uncleaved signal sequence/transmembrane (TM) domain, and a cytoplasmic domain consisting of two α-helices and two highly conserved casein kinase sites (Hout et al., 2004; McCormick-Davis et al., 2000a; Schubert et al., 1994). Previous studies have shown that the Vpu protein has at least two functions within HIV-1 infected cells. The first of these functions involves the interaction of Vpu with the CD4 molecule and subsequent shunting of CD4 to the proteasome for degradation (Fujita et al., 1997; Schubert et al., 1998). Both α-helices as well as the highly conserved

* Corresponding author.
E-mail address: estephen@kumc.edu (E.B. Stephens).

0042-6822/$ - see front matter © 2005 Elsevier Inc. All rights reserved.
doi:10.1016/j.virol.2005.04.038

casein kinase II sites (CK-II) in the region of the cytoplasmic domain have been implicated in the CD4 down-regulation function (Paul and Jabbar, 1997; Schubert et al., 1996b; Tiganos et al., 1998). The second function associated with the Vpu protein is the ability to enhance virion release from infected cells (Klimkait et al., 1990). While the exact mechanism of the enhanced virion release is unknown, some studies have associated this property with the TM of Vpu (Schubert et al., 1996a). The TM of Vpu was shown to form ion channels selective for some monovalent or divalent cations but not to monovalent anions expressed in frog oocytes (Ewart et al., 1996: Schubert et al., 1996a). This ion channel activity was localized to the TM domain and is independent from the cytoplasmic domain in enhancing viral release from cells (Schubert et al., 1996b). More recently, drugs have been identified that will interfere with the Vpu-mediated virion release from cells (Ewart et al., 2002, 2004).

To date, no studies have examined the function of the Vpu transmembrane domain in a relevant animal model of $CD4^+$ T cell loss. The simian-human immunodeficiency virus (SHIV) is a chimeric virus that contains the *tat*, *rev*, *vpu*, and *env* genes in a genetic background of $SIV_{mac}239$. We and others have developed pathogenic SHIVs that are capable of causing profound $CD4^+$ T cell loss and AIDS in both pig-tailed and rhesus macaques (Joag et al., 1996; Luciw et al., 1999; Reimann et al., 1996; Stephens et al., 2002). Our laboratory has been using a pathogenic simian-human immunodeficiency virus (SHIV)/macaque model to examine the role of Vpu in disease (Hout et al., 2004, Singh et al., 2003). Using the pathogenic molecular clone $SHIV_{KU1bMC33}$, we previously showed that an intact Vpu contributed to the $CD4^+$ T cell loss that occurs during infection with the pathogenic SHIV (Stephens et al., 2002) and that disease in macaques only occurred if compensating amino acid substitutions occurred in the Env and Nef proteins (McCormick-Davis et al., 2000b; Singh et al., 2001). In order to study the role the TM plays in vivo to enhance pathogenesis, we constructed a mutant SHIV virus ($SHIV_{TM}$) in which the TM domain of the Vpu protein was scrambled but kept hydrophobic as previously described (Schubert et al., 1996b). In this study, we have analyzed the in vitro replication of this virus and its ability to cause $CD4^+$ T cell loss and disease in macaques. Our results indicate that $SHIV_{TM}$ was not as pathogenic to pig-tailed macaques as the parental $SHIV_{KU1bMC33}$, indicating that the TM domain contributes in part to the rapid $CD4^+$ T cell loss and disease onset caused by $SHIV_{KU1bMC33}$.

Results

The intracellular transport properties of the Vpu_{TM} are the same as the parental subtype B Vpu protein

The sequences of the unmodified and modified Vpu_{TM} proteins are shown in Fig. 1. Before examining the role of Vpu transmembrane domain in pathogenesis, we analyzed the intracellular transport of the modified Vpu_{TM}. To accomplish this, we fused the gene for Vpu_{TM} to the gene of enhanced green fluorescent protein (EGFP) using the same strategy we used to express the unmodified subtype B Vpu (Pacyniak et al., in press; Singh et al., 2003). To examine the intracellular transport, we co-transfected 293 cells with vectors expressing VpuEGFP and Vpu_{TM}EGFP and plasmids expressing an intracellular marker for the Golgi complex (ECFP-Golgi), the rough endoplasmic reticulum (DsRed2-ER), or membranes including the cell plasma membrane (ECFP-Mem). Co-transfection of 293 cells with the vectors expressing the unmodified subtype B Vpu protein (VpuEGFP) and either DsRed2-ER resulted in this protein being partially co-localized with these intracellular markers (Figs. 2A–D). Co-transfection with vectors expressing the unmodified subtype B protein (VpuEGFP) and ECFP-Golgi resulted in almost complete co-localization (Figs. 2E–H). Co-expression of the VpuEGFP with ECFP-Mem revealed that VpuEGFP was not expressed on the cell surface, which is similar to what we previously reported (data not shown). Co-transfection of 293 cells with the vectors expressing Vpu_{TM}EGFP and DsRed2-ER resulted in the partial co-localization of the two proteins (Figs. 2I–L) while co-transfection of 293 cells with vectors expressing Vpu_{TM}EGFP and ECFP-Golgi resulted in almost complete co-localization (Figs. 2M–P). Similar to unmodified protein, co-transfection of 293 cells with a vector expressing the Vpu_{TM}EGFP and ECFP-Mem markers revealed partial co-localization and the Vpu_{TM}EGFP did not appear to be on the cell surface (data not shown). These results indicate that scrambling the amino acids of the transmembrane domain still resulted in a protein that was transported to the same intracellular compartment as the unmodified Vpu protein and correlated well with previous studies (Schubert et al., 1996b) as well as our recent study in which we identified a region within the cytoplasmic domain as having a Golgi retention signal (Pacyniak et al., in press).

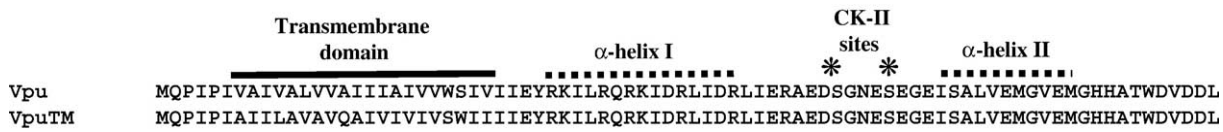

Fig. 1. Sequence of the parental and scrambled Vpu proteins used in this study.

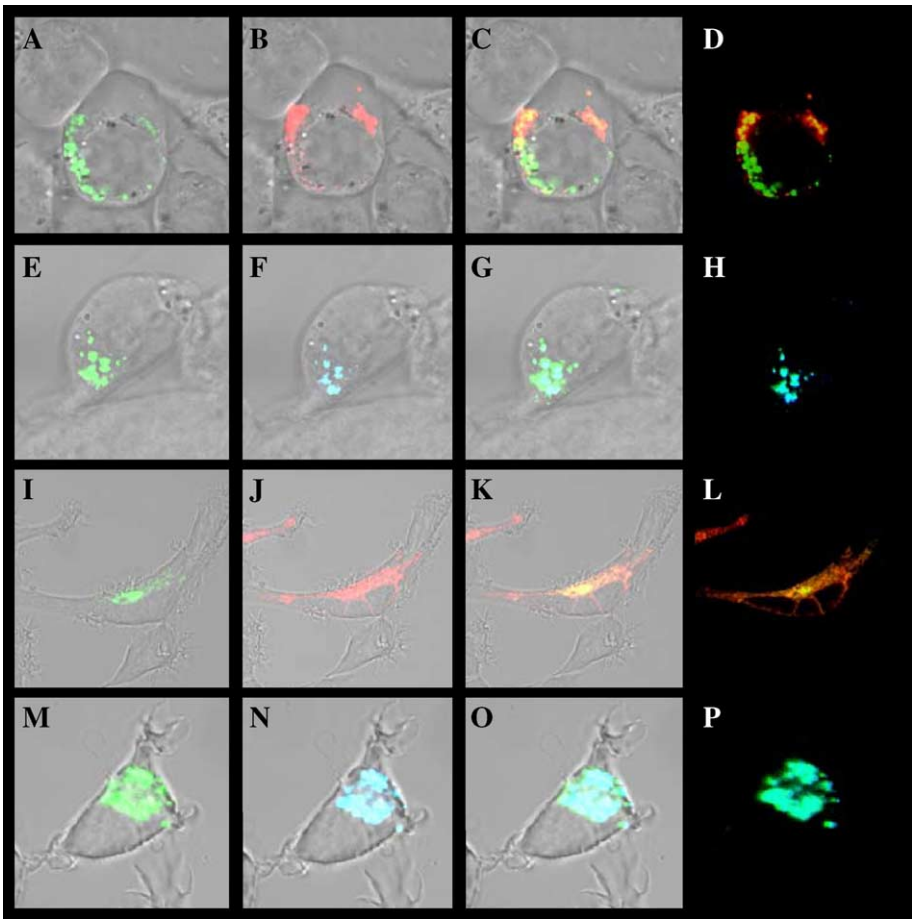

Fig. 2. The Vpu_{TM}EGFP protein is transported to the same intracellular compartment as the unmodified VpuEGFP. 293 cells were co-transfected with vectors expressing the EGFP or VpuEGFP and DsRed2-ER or ECFP-Golgi. At 48 h, cells expressing EGFP and ECFP were examined and images collected using laser scanning confocal microscopy as described in Materials and methods. (Panels A–D) 293 cells co-transfected with vectors expressing VpuEGFP and DsRed2-ER. (Panel A) Expression of VpuEGFP. (Panel B) Expression of DsRed2-ER. (Panel C) Merge of panels A and B. (Panel D) Fluorescence micrograph of EGFP and DsRed2 fusion proteins from panels A and B. (Panels E–H) 293 cells co-transfected with Vpu_{TM}EGFP and ECFP-Golgi. (Panel E) Expression of VpuEGFP. (Panel F) Expression of ECFP-Golgi. (Panel G) Merge of panels E and F. (Panel H) Fluorescence micrograph of EGFP and ECFP fusion proteins from panels E and F. (Panels I–L) 293 cells co-transfected with Vpu_{TM}EGFP and DsRed2-ER. (Panel I) Expression of VpuEGFP. (Panel J) Expression of DsRed2-ER. (Panel K) Merge of panels I and J. (Panel L) Fluorescence micrograph of EGFP and DsRed2 fusion proteins from panels I and J. (Panels M–P) 293 cells co-transfected with Vpu_{TM}EGFP and ECFP-Golgi. (Panel M) Expression of Vpu_{TM}EGFP. (Panel N) Expression of ECFP-Golgi. (Panel O) Merge of panels M and N. (Panel P) Fluorescence micrograph of EGFP and ECFP fusion proteins from panels M and N.

The Vpu_{TM}EGFP does not prevent cell surface expression of CD4

To determine if the Vpu_{TM}EGFP was capable of preventing cell surface expression of CD4, HeLa $CD4^+$ cells were transfected with vectors expressing VpuEGFP, Vpu_{TM}EGFP, and EGFP. At 48 h post-transfection, live cells were stained for cell surface CD4, fixed and examined by confocal microscopy. As shown in Figs. 3A–D, cells expressing EGFP did not prevent CD4 expression while transfection of HeLa $CD4^+$ cells with a vector-expressing VpuEGFP prevented cell surface expression (Figs. 3E–H), which is similar to what we previously reported (Pacyniak et al., in press; Singh et al., 2003). Transfection of HeLa $CD4^+$ cells with the vector-expressing Vpu_{TM}EGFP resulted in 100% of the cells expressing CD4 on the cell surface (Figs. 3I–L). In addition to immunofluorescence studies, we examined the ability of Vpu_{TM}EGFP to promote degradation of CD4. 293 cells were transfected with vectors expressing human CD4 and either VpuEGFP, Vpu_{TM}EGFP, or EGFP. At 48 h post-transfection, cells were radiolabeled for 1 h followed by a chase period of 5 h. The results shown in Fig. 3M show that the VpuEGFP caused degradation of CD4 while the expression of EGFP or Vpu_{TM}EGFP did not result in degradation of CD4. Taken together, these results indicate that scrambling the TM domain of Vpu affected the ability of Vpu to induce the degradation of CD4.

The Vpu protein from $SHIV_{TM}$ is expressed and has a similar M_r on SDS-PAGE

We analyzed the expression of the Vpu protein in C8166 cultures inoculated with parental $SHIV_{KU\text{-}1bMC33}$ or $SHIV_{TM}$. Cultures were inoculated with equivalent amounts

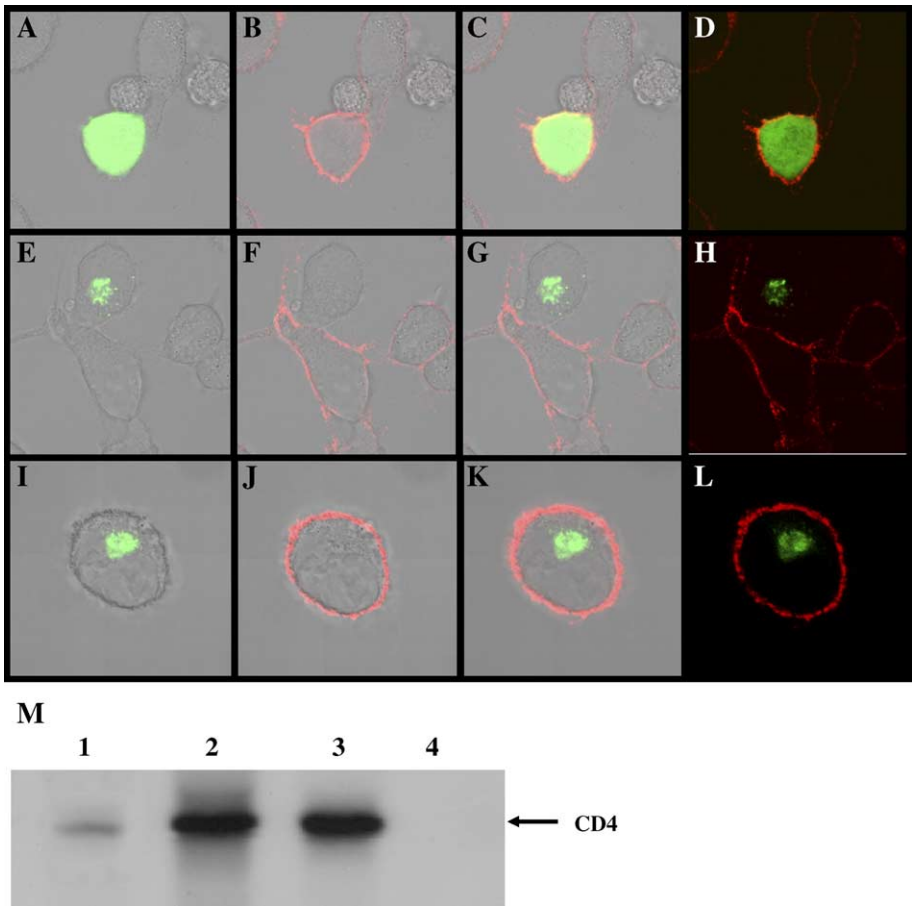

Fig. 3. CD4 down-modulation by EGFP, VpuEGFP, and Vpu_{TM}EGFP proteins. HeLa $CD4^+$ cells, which express CD4, were transfected with vectors expressing EGFP, VpuEGFP, or Vpu_{TM}EGFP. At 48 h post-transfection, cells were stained for surface CD4 using α-CD4 antibody and a rhodamine conjugated secondary antibody followed by fixation with 1% formalin. Cells were examined by laser scanning confocal microscopy. (Panels A, E, and I) Cells examined using a fluorescein filter to visualize EGFP expression and layered onto a phase contrast image of the cell. (Panels B, F, and J) Cells were examined using a rhodamine filter to identify cells expressing the CD4. (Panels C, G, and K) Merge of EGFP and CD4 images (for expression of Vpu fusion protein and CD4 expression). (Panels D, H, and L) Fluorescent micrograph in which the EGFP and CD4 staining are overlayed. (Panels A–D) Cells transfected with a vector-expressing EGFP. (Panels E–H) Cells transfected with a vector-expressing VpuEGFP. (Panels I–L) Cells transfected with a vector-expressing Vpu_{TM}EGFP. (Panel M) The Vpu_{TM}EGFP fusion protein does not induce degradation of human CD4. 293 cells were transfected with vectors expressing human CD4 and either EGFP, VpuEGFP, or Vpu_{TM}EGFP. At 48 h post-transfection, cells were starved for methionine and cysteine and radiolabeled with ^{35}S-methionine/cysteine for 5 h. Cell lysates were prepared in 1× RIPA buffer and the CD4 immunoprecipitated using a rabbit anti-human CD4 antibody and protein A Sepharose (PAS). The immunoprecipitates were washed, boiled in sample reducing buffer and analyzed by SDS-PAGE (10% gel). (Lane 1) CD4 proteins immunoprecipitated from cells co-transfected with vectors expressing human CD4 and VpuEGFP. (Lane 2) CD4 proteins immunoprecipitated from cells co-transfected with vectors expressing human CD4 and Vpu_{TM}EGFP. (Lane 3) CD4 proteins immunoprecipitated from cells co-transfected with vectors expressing human CD4 and EGFP. (Lane 4) CD4 proteins immunoprecipitated from non-transfected cells.

of virus and at 7 days post-inoculation, cells were radiolabeled and Vpu proteins immunoprecipitated from cell lysates. As shown in Fig. 4, a protein with an M_r of 16,000 was immunoprecipitated from $SHIV_{KU\text{-}1bMC33}$-inoculated cultures. A Vpu protein was also immunoprecipitated from $SHIV_{TM}$-inoculated C8166 cultures with similar but not identical mobility by SDS-PAGE, reflecting the difference in the sizes of the two proteins.

The $SHIV_{TM}$ virus is less cytopathic and replicates with decreased kinetics compared to the parental $SHIV_{KU\text{-}1bMC33}$

We compared the kinetics of replication of the $SHIV_{TM}$ with the parental $SHIV_{KU\text{-}1bMC33}$ in C8166 cells. An equivalent number of $TCID_{50}$ were used to inoculate C8166 cells and the culture supernatants analyzed for p27 levels at various times post-inoculation. The results shown in Fig. 5 indicate that the $SHIV_{TM}$ replicated with delayed kinetics compared to the parental $SHIV_{KU\text{-}1bMC33}$ virus. In addition, the cultures of C8166 cells inoculated with $SHIV_{TM}$ exhibited markedly less and delayed syncytial cytopathology compared to cultures inoculated with $SHIV_{KU\text{-}1bMC33}$. Pulse-chase analyses were also performed on infected cultures as we have done in past studies and showed that p27 was released from $SHIV_{TM}$ cultures with delayed kinetics when compared to parental $SHIV_{KU\text{-}1bMC33}$-infected cultures (data not shown). Taken together, these results indicate

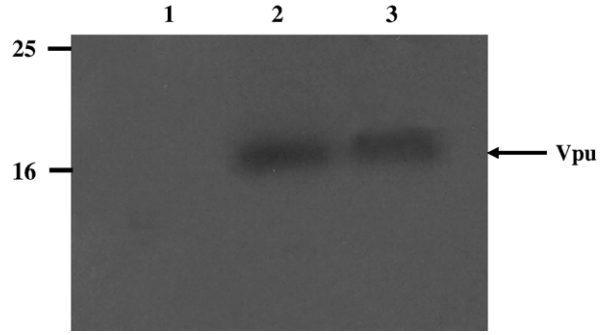

Fig. 4. Immunoprecipitation of Vpu proteins from $SHIV_{KU\text{-}1bMC33}$ and $SHIV_{TM}$-inoculated cultures. C8166 cultures were inoculated with $SHIV_{KU\text{-}1bMC33}$ or $SHIV_{TM}$ at an MOI of approximately 0.01. Cultures were incubated for 6 days and then radiolabeled with ^{35}S-methionine/cysteine for 5 h. Vpu proteins were immunoprecipitated from cell lysates using an α-Vpu serum as described in Materials and methods. A similar number of immunoprecipitated cpm from the $SHIV_{TM}$-inoculated and $SHIV_{KU\text{-}1bMC33}$-inoculated cultures were analyzed under reducing conditions by SDS-PAGE (12.5% gel) and visualized by standard autoradiographic techniques. (Lane 1) Vpu proteins immunoprecipitated from uninoculated cultures. (Lane 2) Vpu proteins immunoprecipitated from $SHIV_{TM}$-inoculated cultures. (Lane 3) Vpu proteins immunoprecipitated from $SHIV_{KU\text{-}1bMC33}$-inoculated cultures. The location of the molecular weight markers is shown on the right.

that the $SHIV_{TM}$ replicated with reduced efficiency compared to the parental $SHIV_{KU\text{-}1bMC33}$.

Electron microscopy reveals that $SHIV_{TM}$ has an altered pattern of maturation in C8166 cells

As the p27 assays revealed that $SHIV_{TM}$ replicated with reduced kinetics compared to the $SHIV_{KU\text{-}1bMC33}$, we examined infected lymphocytes (C8166 cells) by electron microscopy to determine if differences existed in the maturation of $SHIV_{TM}$. As shown in Fig. 6A, C8166 cells inoculated with the $SHIV_{KU\text{-}1bMC33}$ matured at the cell surface of infected cells and is similar to our previous observations (Hout et al., 2004). In contrast, examination of cultures of C8166 cells inoculated with the $SHIV_{TM}$ by electron microscopy revealed fewer particles maturing at the cell plasma membrane (Fig. 6B) although more cells observed with virus within intracellular vesicles and maturing into intracellular vesicles (Fig. 6C). Taken together, these results indicate that the $SHIV_{TM}$ maturation pattern was significantly different from the parental $SHIV_{KU\text{-}1bMC33}$.

The $SHIV_{TM}$ infects pig-tailed macaques but fails to cause the rapid $CD4^+$ T cell loss observed with the parental $SHIV_{KU\text{-}1bMC33}$

To assess the role of the fused *vpu* and *env* genes in $CD4^+$ T cell loss in macaques, three pig-tailed macaques (CX59, CW1K, and CX58) were inoculated with $SHIV_{TM}$. $CD4^+$ T cell counts and viral loads were then monitored over the course of the infections (Fig. 7A). After inoculation with $SHIV_{TM}$, the circulating $CD4^+$ T cell numbers in all three macaques remained in the normal range from 2539 to 4233 cells/μl at week 0 and 1166 to 4033 cells/μl by week 4 post-inoculation, which is a critical time for $CD4^+$ T cell loss in this pathogenic SHIV model. From 4 weeks to 24 weeks, $CD4^+$ T cell numbers remained in the normal range and ranged from 1199 to 2454 cells/μl at 24 weeks post-inoculation. All three macaques were euthanized in apparent good health at 24 or 32 weeks post-inoculation. The circulating $CD4^+$ T cell levels were significantly different to that seen in macaques inoculated with parental $SHIV_{KU\text{-}1bMC33}$, in which a severe drop in the levels of circulating $CD4^+$ T cells within 4 weeks post-inoculation (Fig. 7B).

The plasma viral loads in animals inoculated with $SHIV_{TM}$ were lower compared to the parental $SHIV_{KU\text{-}1bMC33}$

We compared the plasma viral loads in the three macaques inoculated with $SHIV_{TM}$ with the viral loads in macaques inoculated with the parental $SHIV_{KU\text{-}1bMC33}$. As shown in Fig. 7C, all three macaques inoculated with $SHIV_{TM}$ had viral loads that were significantly lower than those from macaques inoculated with the parental $SHIV_{KU\text{-}1bMC33}$ (Fig. 7D).

The sequence of the vpu gene was stable during the course of the macaque infection

In order to assess the stability of the *vpu* gene during the course of infection, DNA was extracted from PBMC samples at 1, 2, 3, 4, 6, 9, 12, 20 weeks, and at necropsy. The *vpu* sequence was amplified, directly sequenced, and compared to the input *vpu* sequence of the $SHIV_{TM}$. No

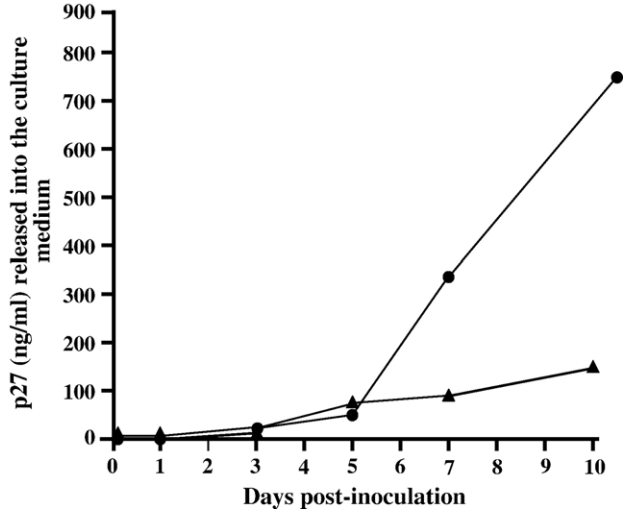

Fig. 5. Growth curves of $SHIV_{KU\text{-}1bMC33}$ and $SHIV_{TM}$ in C8166 cells. Cultures of C8166 cells were inoculate with either $SHIV_{KU\text{-}1bMC33}$ (●) or $SHIV_{TM}$ (▲) as described in the text. Aliquots of the culture medium was assayed for the presence of p27 antigen. The growth curves were performed in triplicate and the mean of the three experiments plotted.

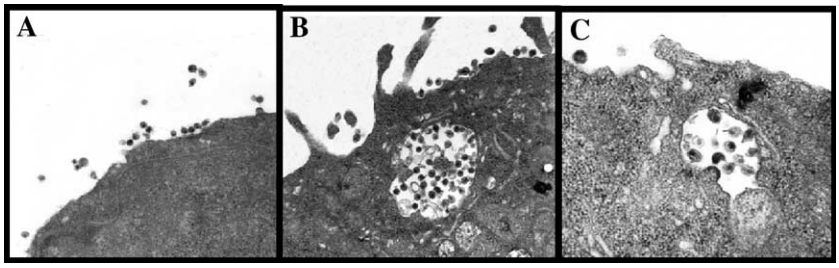

Fig. 6. Examination of the $SHIV_{TM}$ and $SHIV_{KU\text{-}1bMC33}$ maturation by electron microscopy. C8166 cells were inoculated with equivalent amounts of either $SHIV_{TM}$ or $SHIV_{KU\text{-}1bMC33}$ and at 5 days post-inoculation, cells were processed for electron microscopy. (Panel A) Maturation of $SHIV_{KU\text{-}1bMC33}$ showing typical maturation at the cell surface. (Panels B and C) Maturation of $SHIV_{TM}$ showing virus particles at the cell surface and budding into intracellular vesicles.

nucleotide changes were observed in the amplified *vpu* during the course of the infection, indicating that the *vpu* gene was stable (data not shown). We also analyzed the *vpu* sequences analyzed from the mesenteric lymph node, spleen and thymus at necropsy. Sequence analysis revealed that like the PBMC sequences, the *vpu* sequences from the mesenteric lymph node, spleen, and thymus remained stable (data not shown).

Macaques inoculated with $SHIV_{TM}$ exhibited less pathology compared to parental $SHIV_{KU\text{-}1bMC33}$

The distribution of virus in the various visceral tissues was determined by PCR for viral 2-LTR sequences, which is indicative of ongoing replication of the virus. As shown in Table 1, viral 2-LTR sequences were detected in 4 of 13 tissues from CX58, 6 of 13 tissues from CX59, and 4 of 13

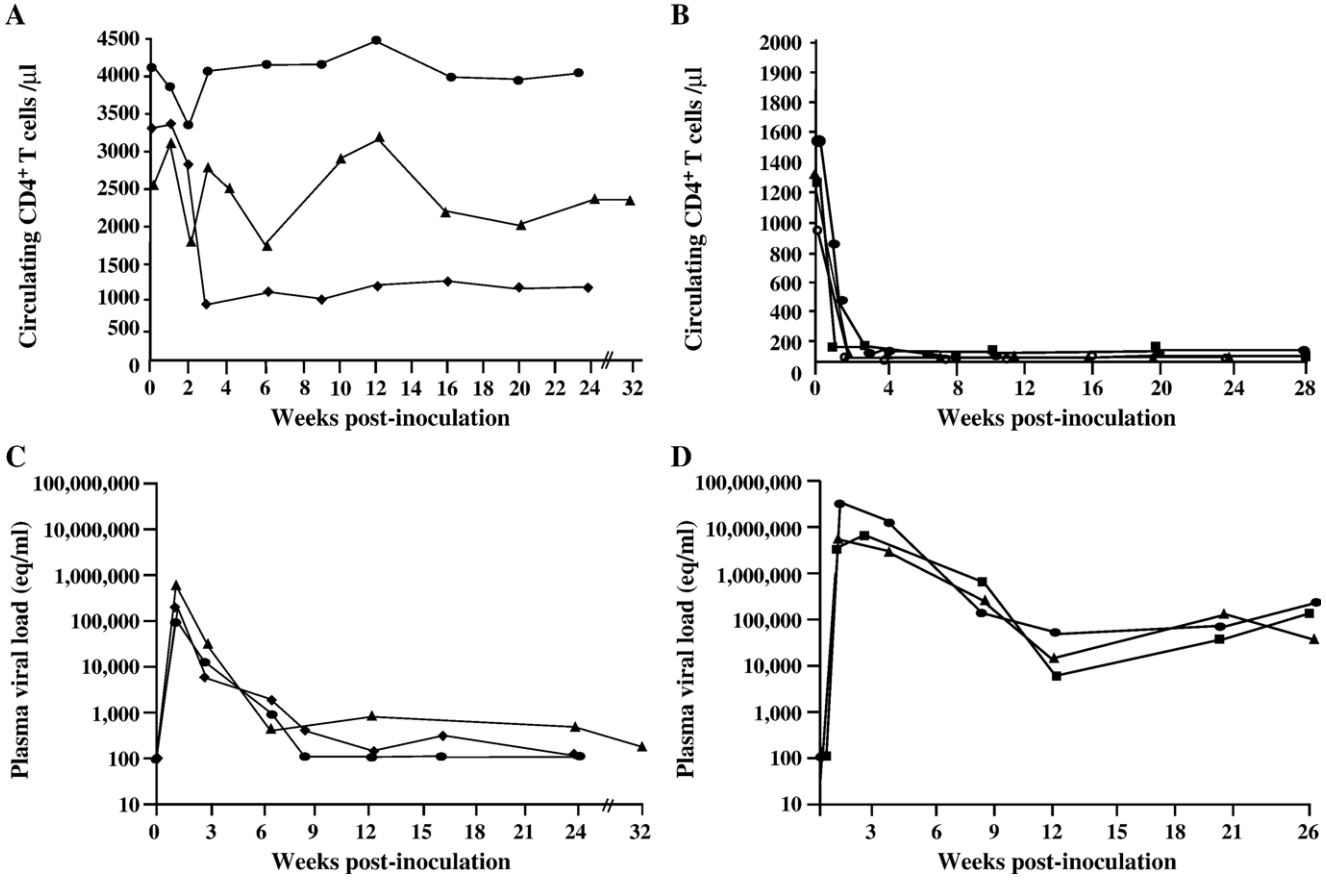

Fig. 7. Circulating $CD4^+$ T cell levels and plasma viral loads following inoculation of macaques with $SHIV_{TM}$ and $SHIV_{KU\text{-}1bMC33}$. (Panel A) The levels of circulating $CD4^+$ T cells in macaques CX58 (●) and CX59 (♦), and CW1K (▲) following inoculation with $SHIV_{TM}$. (Panel B) The levels of circulating $CD4^+$ T cells in four macaques (2000, ●; 2001, ■; CM4G, ○; and CM4K, ▲) following inoculation with $SHIV_{KU\text{-}1bMC33}$. (Panel C) Plasma viral RNA levels in macaques inoculated with $SHIV_{TM}$: CX58 (●), CX59 (♦), and CW1K (▲). (Panel D) Plasma viral RNA levels in three macaques (2000, ●; 2001, ■; and CM4K, ▲) inoculated with $SHIV_{KU\text{-}1bMC33}$. Samples were subjected to real time RT-PCR and Taqman probe homologous to the SIV *gag* gene. Standard curves were generated using five dilutions of viral RNA of known concentration.

Table 1
Distribution of viral 2LTR sequences in tissues from macaques inoculated with $SHIV_{TM}$[a]

Tissue	Macaque		
	CX58	CX59	CW1K
Visceral organs			
Heart	(−)	(−)	(−)
Kidney	(−)	(−)	(−)
Liver	(+)	(−)	(+)
Lung	(−)	(−)	(−)
Pancreas	(−)	(−)	(−)
Salivary gland	(−)	(−)	(−)
Axillary lymph node	(−)	(−)	(−)
Inguinal lymph node	(−)	(+)	(−)
Mesenteric lymph node	(+)	(+)	(+)
Small Intestine	(−)	(+)	(−)
Spleen	(+)	(+)	(+)
Tonsil	(+)	(+)	(+)
Thymus	(−)	(+)	(−)
CNS			
Frontal cortex	(+)	(−)	(−)
Motor cortex	(+)	(+)	(−)
Parietal cortex	(−)	(+)	(−)
Occipital cortex	(−)	(+)	(−)
Temporal cortex	(+)	(−)	(−)
Cerebellum	(−)	(−)	(−)
Medulla	(−)	(+)	(−)
Pons	(−)	(−)	(+)
Midbrain	(−)	(−)	(−)
Thalamus	(−)	(−)	(−)
Corpus callosum	(−)	(−)	(−)
Basal ganglia	(−)	(−)	(−)
Cervical spinal cord	(−)	(−)	(−)
Thoracic spinal cord	(−)	(−)	(−)
Lumbar spinal cord	(−)	(−)	(−)

[a] Tissue DNA samples were analyzed for 2-LTR sequences using nested DNA PCR as described in the text.

tissues from CW1K. The majority of the tissue DNAs that were positive for the presence of 2-LTR sequences were lymphoid organs. We also analyzed the DNA samples isolated from 15 regions of the CNS for *gag* and 2-LTR sequen ces. Macaques CX58, CX59, and CW1K were positive for 2-LTR sequences in 3 of 15, 4 of 15, and 1 of 15 regions of the CNS, respectively (Table 1). Histological examination of lymphoid tissues (inguinal, axillary and mesenteric lymph nodes, small intestine, thymus, tonsil, spleen,) derived from the $SHIV_{TM}$-inoculated macaques revealed no significant lesions within these tissues (Fig. 8). Similarly, no lesions were observed within the brain, heart, kidney, lung, liver, pancreas, and salivary gland (data not shown).

We also compared the number of cells having viral sequences virus from the mesenteric lymph node, spleen and thymus DNA samples isolated at necropsy. As shown in Fig. 9, the numbers of cells containing viral sequences was generally around 10^2 cells per 10^6 cells analyzed. The number of cells producing infectious, cytopathic virus ranged from <10 to 10^2 cells per 10^6 cells analyzed (data not shown), which is lower than what we have reported for parental $SHIV_{KU\text{-}1bMC33}$ (Stephens et al., 2002).

Discussion

Previous studies have shown that the Vpu protein forms an oligomeric structure and modeling studies have suggested that the Vpu ion channel appears to be an oligomer composed of 5 transmembrane spanning α-helices determined by pore radius profiles and conductance predictions (Cordes et al., 2001; Grice et al., 1997; Maldarelli et al., 1993). A role for the TM domain of Vpu in virus pathogenesis and its potential ion channel activity was suggested from a study in which the TM was scrambled but kept hydrophobic (Schubert et al., 1996b). This Vpu protein was found to form an oligomeric structure, was transported to the same intracellular compartments as the unmodified Vpu, down-regulated CD4, but lacked the ion channel activity associated with Vpu (Schubert et al., 1996b). Further, these investigators showed that an HIV-1 virus expressing this Vpu replicated with decreased kinetics and was similar to Vpu-deficient viruses (Schubert et al., 1996b). Using the above scrambled Vpu sequence as the basis for the present study, we constructed a Vpu_{TM}EGFP reporter construct using the same methods used to construct the VpuEGFP (Pacyniak et al., in press; Singh et al., 2003) and showed similar to the VpuEGFP, that the Vpu_{TM}EGFP was localized to the RER and Golgi complex and was not observed to be transported to the cell surface. However, in contrast with a previous study, our Vpu_{TM}EGFP construct did not prevent cell surface expression of CD4. While our results are in contrast with those reported by Schubert et al. (1996b) and we cannot provide an explanation for this discrepancy, our results are consistent with other investigators in the field who showed that the transmembrane domain contains amino acids/structural determinants that affect CD4 down-regulation (Tiganos et al., 1998). We do not believe that the inability of the Vpu_{TM}EGFP to down-regulate CD4 was due to the Vpu fusion to the EGFP as we have also constructed a chimeric Vpu protein in which the TM domain was replaced with the TM domain of the M2 protein of influenza A virus. This construct, Vpu_{M2}EGFP, was capable of CD4 down-regulation (unpublished observations). Furthermore, while VpuEGFP and Vpu_{M2}EGFP were capable of forming oligomeric structures, we did not observe the Vpu_{TM}EGFP to form an oligomeric structure, suggesting that the formation of an oligomeric structure may be necessary for CD4 down-regulation (unpublished observations).

Currently, the only model available for assessing the role of different domains of the Vpu protein in $CD4^+$ T cell loss and pathogenesis uses infection of macaques with a pathogenic SHIV. Previously, we showed that inoculation of macaques with the parental pathogenic $SHIV_{KU\text{-}1bMC33}$ resulted in high virus loads, severe $CD4^+$ T cell depletion

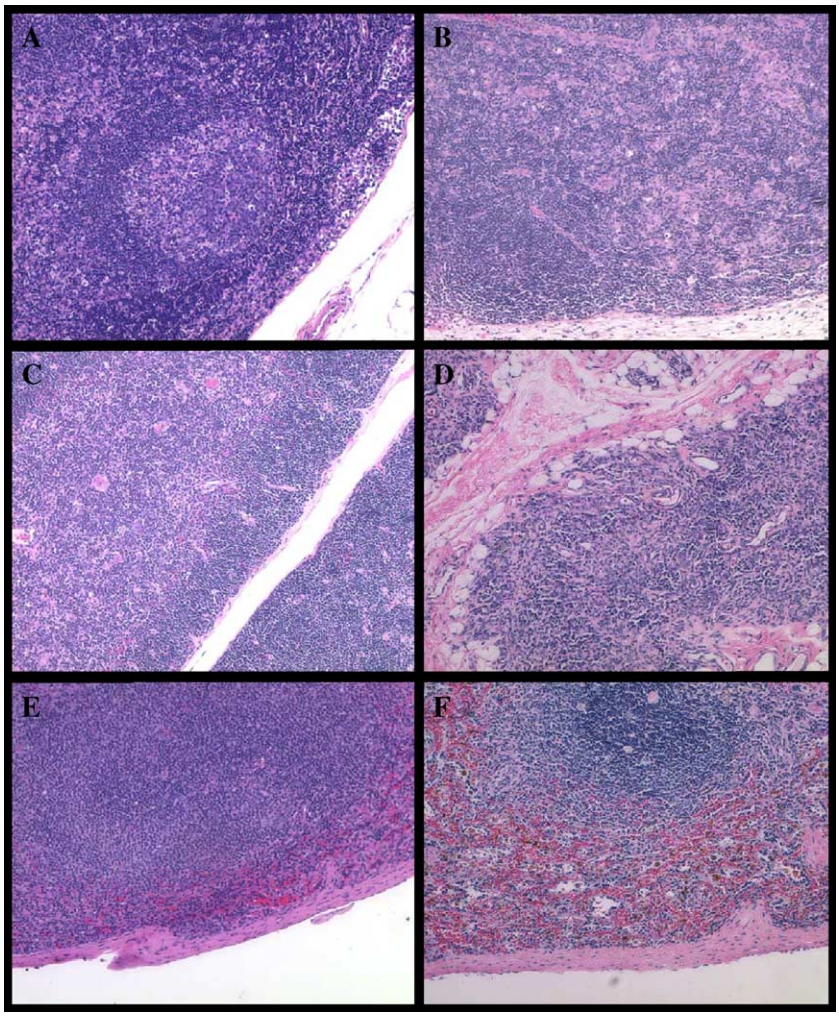

Fig. 8. Pathology associated with $SHIV_{TM}$ infection. Hematoxylin and eosin stains of sections from the mesenteric lymph node (Panels A and B), thymus (Panels C and D) and spleen (Panels E and F) from macaque CX59 (Panels A, C, and E) and an $SHIV_{KU\text{-}1bMC33}$ -inoculated macaque (Panels B, D, and F).

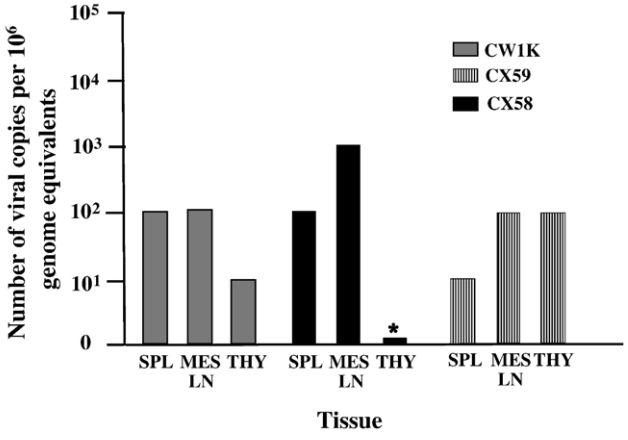

Fig. 9. The number of cells with viral sequences was determined by PCR-ICA as described in the Material and methods section for cells isolated from the mesenteric lymph node (MES), spleen (SPL), and thymus (THY) at necropsy. An (*) indicates that cytopathic virus was not detected.

and lesions consistent with severe lymphoid depletion (Hout et al., 2004; Singh et al., 2003; Stephens et al., 2002). Furthermore, we showed that the Vpu enhances the pathogenicity of $SHIV_{KU\text{-}1bMC33}$ in pig-tailed macaques (Singh et al., 2001; Stephens et al., 2002). Recently, we showed that removal of the highly conserved casein kinase II sites in Vpu from $SHIV_{KU\text{-}1bMC33}$, which previous studies showed were essential to the interaction of Vpu with CD4 (Paul and Jabbar, 1997), contributed to the severe $CD4^+$ T cell loss (Singh et al., 2003). Of the four macaques inoculated with this $SHIV_{S52,56G}$ virus, one developed a severe loss of $CD4^+$ T cells. The one macaque from this study that developed a rapid decline in $CD4^+$ T cells and progression to disease had a reversion of the two casein kinase sites back to the parental $SHIV_{KU1\text{-}bMC33}$ sequence. Using the scrambled TM amino acid sequence from the study described above, we constructed the $SHIV_{TM}$ to assess the role of this domain in the pathogenicity caused by $SHIV_{KU\text{-}1bMC33}$. We hypothesized that the $SHIV_{TM}$ would have similar phenotypic characteristics as previously described (Schubert et al., 1996b).

These include a decrease in virus release in vitro determined by immunoprecipitation of viral proteins, decreased growth replication kinetics determined by p27 growth curves, and differences in virion morphogenesis by electron microscopy. The results of the pulse-chase analysis, p27 growth curves, and electron microscopy indicated that this virus replicated with reduced kinetics when compared to the parental $SHIV_{KU\text{-}1bMC33}$. Electron microscopy revealed viral particles maturing at the cell surface as well as within intracellular vesicles. As our studies indicated that the Vpu_{TM}EGFP did not prevent CD4 down-regulation, we addressed the following question, "Does the TM domain contribute to the pathogenesis of $SHIV_{KU\text{-}1bMC33}$?" Three pig-tailed macaques were intravenously inoculated with $SHIV_{TM}$ and the plasma viral loads, number of infected PBMC, number of PBMC producing infectious virus, and genetic stability of the *vpu* gene were analyzed for over 6 months. All three animals maintained high levels of $CD4^+$ T cells throughout the infection until necropsy. Further viral loads determined by PCR/ICA and RT-PCR showed a significant decrease in the number of infected PBMCs and the ability to recover virus release throughout the infection. Sequence analysis of the *vpu* gene amplified from PBMC at different times after inoculation (1, 2, 3, 4, 6, 9, 12, and 20 weeks as well as at necropsy) revealed that all site-directed changes introduced into the $SHIV_{TM}$Vpu TM were maintained throughout the infection. In addition, we also analyzed the *vpu* sequences from the three lymphoid tissues (mesenteric lymph node, spleen and thymus), which showed that the TM domain sequence was stable in all lymphoid tissues. This is not surprising as 19 nucleotide changes were introduced in the *vpu* gene resulting in 17 amino substitutions. We hypothesize that the lower levels of virus replication in the macaques probably allowed the macaques to develop effective immune responses against the virus to bring replication under control. While we did not examine the host cellular immune responses against the virus, we did examine plasma at necropsy for neutralizing antibodies. All three inoculated macaques developed neutralizing antibodies against the $SHIV_{TM}$ (data not shown). Histopathology of the tissues revealed the absence of lesions characteristic of $SHIV_{KU1bMC33}$ but was similar to the histopathology of non-pathogenic SHIVs (Stephens et al., 2002). Thus, the results presented here, together with our previous results, indicate that both the TM domain and the cytoplasmic domain have structural determinants that contribute to the pathogenicity of $SHIV_{KU\text{-}1bMC33}$.

Although we did not examine the ion channel activity with our $SHIV_{TM}$ as a previous study had shown that this protein had no ion channel activity, we have shown for the first time that by scrambling the amino acids of the TM domain leads to a significant decrease in viral loads and a subsequent decrease in viral pathogenesis. While the mechanism(s) involved in the Vpu-mediated enhanced virus release is currently unknown, it could involve Vpu interaction with a cellular protein or complex of proteins, which facilitates virion release. Evidence in support of this hypothesis has come in a recent study showing Vpu-mediated enhanced viral release from certain human cell lines but not simian cell lines (Varthakavi et al., 2003). Alternatively, the ion channel that has been associated with the Vpu TM domain (Ewart et al., 1996; Park et al., 2003; Schubert et al., 1996a) could modify the local environment of the cell to facilitate release. However, definitive evidence linking the ion channel activity with enhanced virus release or altered virus maturation are still lacking. Studies are underway to determine if replacement of the Vpu TM domain with the TM domain of the M2 protein of the influenza A virus (albeit, with its different ion selectivity), which is the most extensively studied viroporin, would abrogate the effects of a scrambled TM as in $SHIV_{TM}$ and restore the pathogenicity of the virus.

Materials and methods

Cells, plasmids, and viruses

The lymphocyte C8166 cell line was used for transfections as well as indicator cells to measure infectivity and cytopathicity of the viruses used in this study. C8166 cells were maintained in RPMI-1640, supplemented with 10 mM HEPES buffer pH 7.3, 2 mM glutamine, 5 μg per ml gentamicin, and 10% fetal bovine serum. The 293 cell line was maintained in Dulbecco' s minimal essential medium (DMEM) supplemented with 10% fetal bovine serum and 5 μg per ml of gentamicin. The HeLa $CD4^+$ cell line was obtained from the NIH AIDS Research and Reference Reagents Branch and was maintained in RPMI-1640 medium supplemented with 10% fetal bovine serum and 1 mg/ml of Geneticin (Gibco). The derivation of $SHIV_{KU\text{-}1bMC33}$ has been previously described (McCormick-Davis et al., 2000b; Stephens et al., 2002).

Construction of $SHIV_{TM}$

Construction of the $SHIV_{TM}$ virus containing the scrambled transmembrane (TM) domain was accomplished in several steps. Plasmid pUC19)SNvpu12, containing the *Sph*I to *Kpn*I fragment of $SHIV_{KU\text{-}1bMC33}$ in pUC-19 (and coding for the *tat*, *rev*, *vpu* and 5′ end of *env*) was used for the site-directed mutagenesis studies. The plasmid used was pUC19)SNvpu12 and the Quick-Change Mutagenesis Kit (Stratagene) according to the manufacturer's instructions. A total of 19 site directed mutagenesis reactions were performed resulting in 17 amino acids changed in the predicted transmembrane domain (Fig. 1). Clones were isolated, plasmids isolated and the entire insert sequenced to determine if the mutations were introduced as expected and to ensure that no additional changes were introduced during

the mutagenesis step. A plasmid was isolated and designated as pVpu$_{TM}$ that contained the desired mutations. This plasmid was digested to completion with *Sph*I/*Kpn*I, the 450 base pair fragment isolated, and subcloned into the p3′SHIV$_{KU-1bMC33}$ plasmid as previously described (McCormick-Davis et al., 2000a). The resulting plasmid, p3′SHIV$_{TM}$ was used to construct an infectious virus known as SHIV$_{TM}$ using procedures previously described (Liu et al., 1999; McCormick-Davis et al., 2000a; Stephens et al., 1998). Stocks of the virus were prepared and titered in C8166 cells. The virus stock was examined by PCR amplification of the *vpu* gene sequence and sequence analysis to ensure the purity of the stock virus.

Construction of a vector-expressing Vpu$_{TM}$EGFP

In order to examine the intracellular transport and localization of the Vpu with a scrambled TM domain, we constructed a vector that expressed the Vpu$_{TM}$ fused to the gene expressing enhanced green fluorescent protein (EGFP). The procedure for the construction of the Vpu$_{TM}$EGFP was similar to that reported for construction of the VpuEGFP (Pacyniak et al., in press; Singh et al., 2003). The *vpu* gene from SHIV$_{TM}$-infected C8166 cells was amplified by PCR, with oligonucleotides containing flanking *Nco*I sides on either side 5′ and 3′ ends of *vpu*. The 5′ oligonucleotide that was used for amplification was 5′-**CCATG**GCTACAGAT-CATCAACATCCC-3′ (sense), which introduced a *Nco*I site (bolded) within the start codon. The 3′-oligonucleotide that was used for amplification was is 5′-ACCCTACTTCTAC-TAGACAT**GGGTAC**C-3′ (antisense), which introduced a *Nco*I site (bolded) just 3′ to the *vpu* sequence. The PCR product was isolated, cut with the restriction enzyme *Nco*I and was cloned into the pGEMT-Easy vector (Promega) according to the manufacturer's instructions. This plasmid, known as *pvpu*$_{TM}$ *Nco*I, was digested to completion using the restriction endonuclease *Kpn*I and *Nco*I, the *vpu* gene fragment was gel purified and subcloned into *Kpn*I/*Nco*I-digested pEGFP vector (Clontech Laboratories) that has an *Nco*I site at the 5′ end of the *egfp* gene. The resulting plasmid, known as *pvpu*$_{TM}$EGFP, was sequenced to ensure that: (a) the *vpu* gene was inserted in the proper orientation and (b) the junction between the *vpu* and *egfp* genes was in-frame. For expression studies, *pvpu*$_{TM}$EGFP was digested with restriction enzymes *Kpn*I and *Stu*I and sub-cloned into the *Kpn*I and *Eco*RV sites of eukaryotic expression vector pcDNA 3.1(+). This plasmid construct, designated as p*cvpu*$_{TM}$EGFP, was sequenced in its entirety to check for possible sequence changes that may have occurred during the cloning process and used for expression studies in 293 cells.

Transfections and laser scanning confocal fluorescence microscopy analysis

Plasmid vectors expressing VpuEGFP, Vpu$_{TM}$EGFP and EGFP proteins were transfected in human 293 cells to assess their subcellular localization using a cationic polymer (polyethylenimine) transfection reagent (ExGen 500, MBI Fermentas) following the manufacturer's protocol. Briefly, $1-3 \times 10^5$ cells were seeded onto cover slips in each well of a 6 well tissue culture plate 24 h prior to transfection. Transfection was carried out on cultures that were 50–60% confluent using 4.75 μg plasmid DNA and 15.5 μl of ExGen 500 corresponding to 5 equivalents. Each plasmid DNA sample was diluted in 300 μl of 150 mM sodium chloride solution separately. Samples were vortexed gently and immediately centrifuged at low revolution for a few seconds. Polyethylenimine was then added to the plasmid DNA solution, mixed with a vortex and allowed to stand at room temperature for 10 min. The 293 cells were washed with serum-free media twice and 3.0 ml of serum-free DMEM was added. The polyethylenimine/DNA mixture was added to the cells and the plate swirled by slow hand rotation for a couple of seconds. Culture plates were centrifuged at 280×*g* for 5 min and incubated at 37 °C for 30 min. The medium from transfected cultures was replaced with fresh complete growth media and cells were incubated at 37 °C in 5% CO_2 atmosphere.

Transfected cells were observed by confocal microscopy, which is known to have the advantage that fluorescence can be detected from cells in different optical sections. Transfected cells were grown in 35 mm Petri dishes, and were prepared for confocal microscopy as follows. Cells were rinsed briefly in phosphate buffered saline (PBS, pH 7.2) at room temperature. The cells were fixed in freshly prepared, ice cold, 1% paraformaldehyde in 0.13M sodium phosphate pH 7.2 for 2 min. The fixative was removed and the cells briefly rinsed in phosphate buffered saline. The saline was removed, and one drop of mounting media was placed on each dish. The mounting media is composed of 75% glycerol, 25% 0.13 M sodium phosphate buffer pH 8.0 plus 0.02% n-propyl gallate. A square number one glass cover slip was placed over each dish. The cells were imaged with a Zeiss LSM 510 confocal microscope in the upright configuration. The objective used was a 63 × 1.4 n.a. Plan Apochromat. Images were captured at 12 bit resolution with a pixel array of 1024 × 1024 and a zoom of 2.0×. The signal was averaged 4 times per line. The EGFP was excited with light at 488 nm (laser intensity 75% for all images), and the emitted light was collected after passing through a 505-nm long pass filter. The amplifier offset and gain were identical for all images. The SC detector gain was decreased from 692 nm to 618 nm for cells expressing Vpu EGFP1 since the intensity of the signal resulted in saturation. A Z stack of 20 optical slices was obtained so that the entire cell was imaged from bottom to top. The pinhole was set to 96 μm which at this wavelength represents one airy unit. The optical section had a width of 0.7 μm. Simultaneous to the acquisition of the confocal signal from the EGFP, a non-confocal transmitted light image was obtained to provide a reference point for the

EGFP signal. Individual confocal slices were overlaid onto the greyscale transmitted light image.

To confirm the presence of the Vpu fusion protein at different subcellular compartments, a series of co-transfection studies were performed using vectors expressing either an ER marker fused to the fluorescent protein DsRed2 (DsRed2-ER), a Golgi complex marker fused to a cyano-variant of EGFP (pECFP-Golgi), or a membrane marker fused to a cyano-variant of EGFP (pECFP-Mem). 293 cells were co-transfected with vectors expressing the various Vpu fusion proteins and either DsRed2-ER, ECFP-Golgi, or ECFP-Mem. At 48 h post-transfection, cells were processed for confocal microscopy as described above, and cells identified expressing both proteins. Fluorescent digital images were obtained using a Zeiss LSM510 confocal microscope equipped with an Argon/2 laser (25 mW) for the excitation (488 nm, 50% laser power) and detection (band pass 505–530 nm filter; BP505–530) of EGFP, for the excitation (458 nm, 100% laser power) and detection (band pass 475–525 nm filter; BP475–525) of ECFP, and for excitation (558 nm, 100% laser power) and detection (band pass 583 nm filter; LP560) of DsRed2. Images were acquired in Multitrack channel mode (sequential excitation/emission) with LSM510 (v 3.2) software and a Plan-Apochromat 100 ×/1.4 Oil DIC objective with frame size of 1024 × 1024 pixels. Detector gain was set initially to cover the full range of all the samples and background corrected by setting the amplifier gain, and all images were then collected under the same photomultiplier detector conditions and pinhole diameter.

Assays for detection of cell surface CD4 and degradation of CD4

To determine if the Vpu_{TM}EGFP construct was capable of promoting degradation of CD4 in transfected cells, we employed HeLa $CD4^+$ cells. Cultures of HeLa $CD4^+$ in which approximately 80–85% of the cells stained positive for surface CD4 were re-cloned to obtain a population of cells in which >99% of the cells stained positive for cell surface CD4. Briefly, HeLa $CD4^+$ cells were grown on cover slips and transfected with p*cvp*uEGFP as described earlier. At 48 h post-transfection, cells were washed twice with wash buffer (PBS pH 7.2, containing 2% fetal calf serum and 0.01% NaN_3) and reacted with mouse anti-CD4 (clone SFCI12T4D11CD4, Beckman-Coulter, 1:500 dilution) for 45 min. After the incubation, cover slips were washed three times and incubated with rhodamine-conjugated secondary antibody (goat anti-mouse, Chemicon, 1:50 dilution) for 35 min followed by washing five times in buffer without serum. Cells were then fixed in 1% formalin for 10 min, washed twice, equilibrated with anti-fade buffer and mounted on microscope glass slides using Anti-fade (Molecular Probes, Oregon). Cells were immediately observed under a fluorescent microscope (Nikon TE300) with fluorescein filter (for visualization of EGFP) and rhodamine filters (for visualization of CD4 staining). All the staining procedures were performed on ice and in the dark. HeLa $CD4^+$ cells transfected with EGFP alone served as control for down-regulation of CD4 and cultures of HeLa $CD4^+$ cells treated with wash buffer instead of primary antibody served as negative control for CD4 staining. A minimum of 400 EGFP-expressing cells were counted.

In addition to detection of CD4 on the cell surface of transfected HeLa $CD4^+$ cells, co-transfection experiments were performed using vectors expressing either VpuEGFP, Vpu_{TM}EGFP, or EGFP and a vector expressing the human CD4 protein (pCMV4Neo; Goldsmith et al., 1995). Cells were transfected with Vpu fusion proteins and pCMV4Neo vectors at a 3:1 ratio, respectively. This was to insure that all cells transfected with the CD4-expressing vector were also transfected with the vector expressing the Vpu fusion proteins. At 48 h post-transfection, cells were starved for methionine and then radiolabeled with 500 μCi ^{35}S-methionine/cysteine for 1 h. The radiolabel was removed and chased with 100 × cold methionine/cysteine for 4 h. Cells were lysed in RIPA buffer, lysates prepared and the CD4 immunoprecipitated using a rabbit anti-CD4 (sc-7219; Santa Cruz Biotechnology) and protein A Sepharose (PAS). Immunoprecipitates were collected, washed three times with 1 × RIPA and analyzed by SDS-PAGE (10% gel). The negative controls for this study was co-transfection with a vector-expressing EGFP and the positive control was co-transfection with a vector-expressing VpuEGFP (expressing the unmodified subtype B Vpu).

p27 assays

Growth curves based on extracellular release of viral p27 protein were performed on $SHIV_{KU\text{-}1bMC33}$ and $SHIV_{TM}$ virus stocks. Virus stocks were tittered by performing a series of ten fold dilutions in medium without serum and then inoculating a Ghost $CD4^+$ cell line, which expresses the green fluorescent protein (GFP) under the control of the HIV-1 LTR. At 48 h post-inoculation, the number of fluorescent cells (indicative of infection by the virus and subsequent expression of the GFP) were scored and titers determined. Cultures of 10^6 C8166 cells were inoculated with equivalent amounts of infectious cell-free virus (1×10^3) for 4 h. At the end of 4 h, the cells were centrifuged at $400 \times g$ for 10 min, the supernatant removed and the cell pellet washed with 10 ml of medium. This was repeated two additional times. The cells were resuspended in RPMI-1640 supplemented with 10% FBS and antibiotics; this was considered as the 0 time point of the assay. Cultures were incubated at 37 °C and aliquots of the culture were removed at 0, 1, 3, 5, 7, and 10 days with fresh media added to cultures at days 3, 5, and 7. The culture medium was removed, cells pelleted by

centrifugation at 300×*g* for 10 min, and assayed for p27 using antigen capture assays (Coulter) according to the manufacturer's instructions.

Electron microscopy

Infected cells were examined by electron microscopy to determine the site of maturation. Cultures of C8166 cells were inoculated with $SHIV_{KU\text{-}1bMC33}$ or $SHIV_{TM}$ at a multiplicity of infection of 0.01. Cells were incubated for a total of 5 days at which time cells were centrifuged at 400×*g* for 10 min. Cells were washed three times with 10 ml of phosphate buffered saline (pH 7.4) and fixed in 2% glutaraldehyde in 0.1 M cacodylate buffer (pH 7.4) overnight at 4 °C. Cells were postfixed in 1% osmium tetroxide (OsO_4) for 1 h, cells washed twice with water and dehydrated through a series of alcohols (30–100%) and the cells were embedded in Embed 812 resin. Thin sections were cut at 80 A, stained with uranyl acetate and lead citrate and examined under a JEOL 100CXII transmission electron microscope. For enumeration of virus particles on the surface of cells, C8166 cultures were inoculated with equivalent amounts of each virus for 5 days and cultures processed as described above. The number of particles associated with 50 different cells was determined and the mean number of particles calculated per infected cell.

Macaques analyzed in this study

Three 1–1.5 year old pig-tailed macaques (*Macaca nemestrina*; CX59, CX58, CW1K) were inoculated intravenously with 1 ml of undiluted supernatant from C8166-grown stocks of virus containing 10^4 $TCID_{50}$ per milliliter. These macaques were euthanized at 24–32 weeks following inoculation. The inoculated macaques were compared to macaques inoculated with $SHIV_{KU\text{-}1bMC33}$ (pathogenic virus) and those inoculated with n*ovp*uSH-$IV_{KU1bMC33}$ as previously described (Hout et al., 2004; Singh et al., 2003; Stephens et al., 2002). The animals were housed in the AAALAC-approved animal facility at the University of Kansas Medical Center. Heparinized blood was collected weekly for the first 4 weeks, then at 2-week intervals for the next month, and thereafter at monthly intervals.

Assays for circulating $CD4^+$ T cells

Alterations in the levels of $CD4^+$ lymphocytes after experimental inoculations were monitored sequentially by FACS analysis (Becton Dickinson). T lymphocyte subsets were labeled with OKT4 (CD4; Ortho Diagnostics Systems, Inc), SP34 (CD3; Pharmingen) or FN18 (CD3; Biosource International) monoclonal antibodies. T lymphocyte subsets from a normal uninfected macaque were always performed at the same time as inoculated macaques as a control for the FACS analysis.

Processing of tissue samples at necropsy

At the time of euthanasia, all animals in this study were anesthetized by administration of 10 mg/kg ketamine (IM) followed by an intravenously administration of sodium phenobarbital at 20–30 mg/kg. A laparotomy was performed and the animal exsanguinated by aortic cannulation and perfused with one liter of cold Ringer's saline. All aspects of the animal studies were performed according to the institutional guidelines for animal care and use at University of Kansas Medical Center. Lymphoid tissues (lymph nodes, spleen, and thymus) and non-lymphoid tissues (brain, heart, kidneys, liver, lung, pancreas, small intestine) were obtained and aliquots of tissue snap frozen for DNA and RNA assays. Portions of lymphoid tissues were immersed in Hank's buffered saline (HBSS) to quantitate levels of infectious virus in tissues.

Sequence analysis of the vpu gene

The *vpu* gene was amplified from several tissue DNA samples taken at necropsy to examine if the sequence of *vpu* was stable. For amplification of the *vpu*, we used oligonucleotide primers 5′-CCTAGACTAGAGCCCTGGAAGCATCC-3′ (sense) and 5′-GTACCTCTGTATCATATGCTTTAGCAT-3′ (antisense), which are complementary to nucleotides 5845–5870 and 6393–6420 of the HIV-1 (HXB2) genome, respectively (Ratner et al., 1985). One microgram of genomic DNA was used in the PCR with Taq DNA polymerase and the conditions described above. For the second round of amplification, we used oligonucleotide primers 5′-TTAGGCATCTCCTATGGCAGGAAGAAG -3′ (sense) and 5′CACAAAATAGAGTGGTGGTTGCTTCCT-3′ (antisense), which are complementary to nucleotides 5956–5984 and 6386–6413 of the HIV-1 (HXB2) genome (Ratner et al., 1985), respectively. The conditions for amplification were identical to those described above. For sequence analysis, the PCR products from three separate PCRs were separated by electrophoresis in a 1% agarose gel, isolated, and molecularly cloned into the pGEM-T Easy vector according to the manufacturer's instructions. Cycle sequencing reactions using the BigDye Terminator Cycle Sequencing Ready Reaction Kit with AmpliTaq DNA polymerase, FS (PE Applied Biosystems, Foster City, CA) and sequence detection was conducted with an Applied Biosystems 377 Prism XL automated DNA sequencer and visualized using the ABI Editview program. Sequences were compared to the intact sequences from $SHIV_{KU\text{-}1bMC33}$.

PCR amplification of viral sequence from tissues

SHIV gag

DNA extracted from the visceral organs and different regions of the CNS as previously described (McCormick-Davis et al., 2000b) were used to amplify viral *gag*

sequences. The oligonucleotides used for the first round of amplification were 5′-GATGGGCGTGAGAAACTCCG-TCTT-3′ (sense) and 5′-CCTCCTCTGCCGCTAGATGGT-GCTGTTG-3′ (antisense) corresponding to the region 1052–1075 and 1423–1450 of the $SIV_{mac}239$ *gag* gene respectively (Regier and Desrosiers, 1990). The nested $SIV_{mac}239$ primers used were 5′-GAACATGTTGAAGCATGTAG-TATGGGCAGC-3′ (sense) and 5′-CACCACTAGGTGTC-TCTGCACTATCTGTTTTGC-3′ (antisense) which are complementary to bases 1142–1165 and 1356–1382 of $SIV_{mac}239$, respectively.

Long terminal repeat circles

We examined tissue DNA samples for the presence of 2-LTR circular DNA as it provides a view of a spreading infection based on a viral DNA form that is structurally distinct and known to have a short half-life in infected cells (Sharkey and Stevenson, 2001; Sharkey et al., 2000; Teo et al., 1997; Zazzi et al., 1997). DNA isolated from visceral organs and 12 regions of the brain was analyzed for the presence of 2-LTR circular forms of DNA as previously described (McCormick-Davis et al., 2000b). The oligonucleotides used in the first round were 5′-CCTCCTGTGCCTCATCTGATACATTTAC-3′ (U5 region) and 5′-ATTTCGCTCTGTATTCAGTCGCTCTGC-3′ (U3 region), which correspond to bases 10,335 to 10,361 and 180 to 153 of the SHIV genome, respectively. The PCR amplification was performed using the following conditions: denaturation at 92 °C for 1 min, annealing at 55 °C for 1 min, and primer extension at 72 °C for 3 min. One microliter of the first PCR product was used as a template for a second amplification using the same conditions. The oligonucleotides primers used for the second round were 5′-TTGGGTATCTAATTCCTGGTCCTGAG-3′ (U5 region) and 5′-AGGTTCTCTCCAGCACTAGCAGG-TAGAGC-3′ (U3 region; opposite strand; 456), which corresponds to bases 10,389 to 10,417, and 120 to 95 of the SHIV genome, respectively. The predicted product of the 2-LTR PCR product is 361 base pairs.

Analysis of virus loads in macaques

PCR-ICA

The virus loads in the CNS and lymphoid tissues were determined using a quantitative PCR assay modified from a PCR-infected cell assay previously described (Joag et al., 1994; Stephens et al., 1998). In this assay, 1 μg of total cellular DNA isolated from tissues was subjected to a series of 10-fold dilutions such that samples contained from 100 ng to 10 fg (less than one copy of chromosomal DNA). These samples were used in nested PCR reactions that amplified either the β-actin gene of the cell (a single copy gene) or the *gag* gene from $SHIV_{KU1bMC33}$. Amplification of either gene using the primers previously described was shown to detect one of the copy of each gene (Joag et al., 1994). Thus, amplification of the β-actin gene determined the number of genome equivalents in each sample, whereas amplification with the gag primers determined the number of viral copies per number of genome equivalents. The values were expressed as the number of viral copies per 10^6 genome equivalents.

Plasma virus loads

Plasma viral RNA loads were determined on RNA extracted from 500 μl of EDTA-treated plasma. Virus was pelleted and RNA extracted using the Qiagen viral RNA kit (Qiagen, Valencia, CA). RNA samples were analyzed by real-time RT-PCR using *gag* primers and a 5′FAM and 3′TAMRA labeled Taqman probe that was homologous to the SIV *gag* gene as previously described (Hofmann-Lehmann et al., 2000). Standard curves were prepared using a series of six 10-fold dilutions of viral RNA of a known concentration. The sensitivity of the assay was 100 RNA equivalents per ml. Samples were analyzed in triplicate and the number of RNA equivalents were calculated per ml of plasma.

Acknowledgments

The work reported here is supported by grants NIH grants AI51981 and AA13845 to E.B.S. and RR00163 to S.W.W The anti-Vpu serum and HeLa $CD4^+$ cells were provided by the NIH AIDS Research and Reference Reagent Program.

References

Cordes, F.S., Kukol, A., Forrest, L.R., Arkin, I.T., Sansom, M.S., Fischer, W.B., 2001. The structure of the HIV-1 Vpu ion channel: modelling and simulation studies. Biochim. Biophys. Acta 1512, 291–298.

Ewart, G.D., Sutherland, T., Gage, P.W., Cox, G.B., 1996. The Vpu protein of human immunodeficiency virus type 1 forms cation-selective ion channels. J. Virol. 70, 7108–7115.

Ewart, G.D., Mills, K., Cox, G.B., Gage, P.W., 2002. Amiloride derivatives block ion channel activity and enhancement of virus-like particle budding caused by HIV-1 protein Vpu. Eur. Biophys. J. 31, 26–35.

Ewart, G.D., Nasr, N., Naif, H., Cox, G.B., Cunningham, A.L., Gage, P.W., 2004. Potential new anti-human immunodeficiency virus type 1 compounds depress virus replication in cultured human macrophages. Antimicrob. Agents Chemother. 48, 2325–2330.

Fujita, K., Omura, S., Silver, J., 1997. Rapid degradation of CD4 in cells expressing human immunodeficiency virus type 1 Env and Vpu is blocked by proteasome inhibitors. J. Gen. Virol. 78, 619–625.

Goldsmith, M.A., Warmerdam, M.T., Atchison, R.E., Miller, M.D., Greene, W.C., 1995. Dissociation of the CD4 down-regulation and viral infectivity enhancement functions of human immunodeficiency virus type 1 Nef. J. Virol. 69, 4112–4121.

Grice, A.L., Kerr, I.D., Sansom, M.S., 1997. Ion channels formed by HIV-1 Vpu: a modelling and simulation study. FEBS Lett. 405, 299–304.

Hofmann-Lehmann, R., Swenerton, R.K., Liska, V., Leutenegger, C.M., Lutz, H., McClure, H.M., Ruprecht, R.M., 2000. Sensitive and robust one-tube real-time reverse transcriptase-polymerase chain reaction to quantify SIV RNA load: comparison of one- versus two-enzyme systems. AIDS Res. Hum. Retroviruses 16, 1247–1257.

Hout, D.R., Mulcahy, E.R., Pacyniak, E., Gomez, L.M., Gomez, M., Stephens, E.B., 2004. Vpu: A multifunctional protein that enhances the pathogenesis of human immunodeficiency virus type 1. Cur. HIV-1 Res. 2, 255–270.

Joag, S.V., Stephens, E.B., Adams, R.J., Foresman, L., Narayan, O., 1994. Pathogenesis of SIVmac infection in Chinese and Indian rhesus macaques: effects of splenectomy on virus burden. Virology 200, 436–446.

Joag, S.V., Li, Z., Foresman, L., Stephens, E.B., Zhao, L.J., Adany, I., Pinson, D.M., McClure, H.M., Narayan, O., 1996. Chimeric simian/human immunodeficiency virus that causes progressive loss of $CD4^+$ T cells and AIDS in pig-tailed macaques. J. Virol. 70, 3189–3197.

Klimkait, T., Strebel, K., Hoggan, M.D., Martin, M.A., Orenstein, J.M., 1990. The human immunodeficiency virus type 1-specific protein vpu is required for efficient virus maturation and release. J. Virol. 64, 621–629.

Liu, Z.Q., Muhkerjee, S., Sahni, M., McCormick-Davis, C., Leung, K., Li, Z., Gattone, V.H., Tian, C., Doms, R.W., Hoffman, T.L., Raghavan, R., Narayan, O., Stephens, E.B., 1999. Derivation and biological characterization of a molecular clone of SHIV(KU-2) that causes AIDS, neurological disease, and renal disease in rhesus macaques. Virology 260, 295–307.

Luciw, P.A., Mandell, C.P., Himathongkham, S., Li, J., Low, T.A., Schmidt, K.A., Shaw, K.E., Cheng-Mayer, C., 1999. Fatal immunopathogenesis by SIV/HIV-1 (SHIV) containing a variant form of the HIV-1SF33 env gene in juvenile and newborn rhesus macaques. Virology 263, 112–127.

Maldarelli, F., Chen, M.Y., Willey, R.L., Strebel, K., 1993. Human immunodeficiency virus type 1 Vpu protein is an oligomeric type I integral membrane protein. J. Virol. 67, 5056–5061.

McCormick-Davis, C., Dalton, S.B., Singh, D.K., Stephens, E.B., 2000a. Comparison of Vpu sequences from diverse geographical isolates of HIV type 1 identifies the presence of highly variable domains, additional invariant amino acids, and a signature sequence motif common to subtype C isolates. AIDS Res. Hum. Retroviruses 16, 1089–1095.

McCormick-Davis, C., Dalton, S.B., Hout, D.R., Singh, D.K., Berman, N.E., Yong, C., Pinson, D.M., Foresman, L., Stephens, E.B., 2000b. A molecular clone of simian-human immunodeficiency virus (ΔvpuSHIV$_{KU\text{-}1bMC33}$) with a truncated, non-membrane-bound vpu results in rapid $CD4^+$ T cell loss and neuroAIDS in pig-tailed macaques. Virology 272, 112–126.

Pacyniak, E., Gomez, M.L., Mulcahy, E.R., Jackson, M.J., Hout, D.R., Wisdom, B.J., Stephens, E.B., in press. Identification of a region within the cytoplasmic domain of the subtype B Vpu protein of human immunodeficiency virus type 1 (HIV-1) that is responsible for retention in the Golgi complex and its absence in the Vpu protein from subtype C HIV-1. AIDS Res. Hum. Retro.

Park, S.H., Mrse, A.A., Nevzorov, A.A., Mesleh, M.F., Oblatt-Montal, M., Montal, M., Opella, S.J., 2003. Three-dimensional structure of the channel-forming trans-membrane domain of virus protein "u" (Vpu) from HIV-1. J. Mol. Biol. 333, 409–424.

Paul, M., Jabbar, M.A., 1997. Phosphorylation of both phosphoacceptor sites in the HIV-1 Vpu cytoplasmic domain is essential for Vpu-mediated ER degradation of CD4. Virology 232, 207–216.

Ratner, L., Haseltine, W., Patarca, R., Livak, K.J., Starcich, B., Josephs, S.F., Doran, E.R., Rafalski, J.A., Whitehorn, E.A., Baumeister, K., et al., 1985. Complete nucleotide sequence of the AIDS virus, HTLV-III. Nature 313, 277–284.

Regier, D.A., Desrosiers, R.C., 1990. The complete nucleotide sequence of a pathogenic molecular clone of simian immunodeficiency virus. AIDS Res. Hum. Retroviruses 6, 1221–1231.

Reimann, K.A., Li, J.T., Voss, G., Lekutis, C., Tenner-Racz, K., Racz, P., Lin, W., Montefiori, D.C., Lee-Parritz, D.E., Lu, Y., Collman, R.G., Sodroski, J., Letvin, N.L., 1996. An env gene derived from a primary human immunodeficiency virus type 1 isolate confers high in vivo replicative capacity to a chimeric simian/human immunodeficiency virus in rhesus monkeys. J. Virol. 70, 3198–3206.

Schubert, U., Henklein, P., Boldyreff, B., Wingender, E., Strebel, K., Porstmann, T., 1994. The human immunodeficiency virus type 1 encoded Vpu protein is phosphorylated by casein kinase-2 (CK-2) at positions Ser52 and Ser56 within a predicted alpha-helix-turn-alpha-helix-motif. J. Mol. Biol. 236, 16–25.

Schubert, U., Ferrer-Montiel, A.V., Oblatt-Montal, M., Henklein, P., Strebel, K., Montal, M., 1996a. Identification of an ion channel activity of the Vpu transmembrane domain and its involvement in the regulation of virus release from HIV-1-infected cells. FEBS Lett. 398, 12–18.

Schubert, U., Bour, S., Ferrer-Montiel, A.V., Montal, M., Maldarell, F., Strebel, K., 1996b. The two biological activities of human immunodeficiency virus type 1 Vpu protein involve two separable structural domains. J. Virol. 70, 809–819.

Schubert, U., Anton, L.C., Bacik, I., Cox, J.H., Bour, S., Bennink, J.R., Orlowski, M., Strebel, K., Yewdell, J.W., 1998. CD4 glycoprotein degradation induced by human immunodeficiency virus type 1 Vpu protein requires the function of proteasomes and the ubiquitin-conjugating pathway. J. Virol. 72, 2280–2288.

Sharkey, M.E., Stevenson, M., 2001. Two long terminal repeat circles and persistent HIV-1 replication. Curr. Opin. Infect. Dis. 14, 5–11.

Sharkey, M.E., Teo, I., Greenough, T., Sharova, N., Luzuriaga, K., Sullivan, J.L., Bucy, R.P., Kostrikis, L.G., Haase, A., Veryard, C., Davaro, R.E., Cheeseman, S.H., Daly, J.S., Bova, C., Ellison III, R.T., Mady, B., Lai, K.K., Moyle, G., Nelson, M., Gazzard, B., Shaunak, S., Stevenson, M., 2000. Persistence of episomal HIV-1 infection intermediates in patients on highly active anti-retroviral therapy. Nat. Med. 6, 76–81.

Singh, D.K., McCormick, C., Pacyniak, E., Lawrence, K., Dalton, S.B., Pinson, D.M., Sun, F., Berman, N.E., Calvert, M., Gunderson, R.S., Wong, S.W., Stephens, E.B., 2001. A simian human immunodeficiency virus with a nonfunctional Vpu (vpuSHIV$_{KU\text{-}1bMC33}$) isolated from a macaque with neuroAIDS has selected for mutations in env and nef that contributed to its pathogenic phenotype. Virology 282, 123–140.

Singh, D.K., Griffin, D.M., Pacyniak, E., Jackson, M., Werle, M.J., Wisdom, B., Sun, F., Hout, D.R., Pinson, D.M., Gunderson, R.S., Powers, M.F., Wong, S.W., Stephens, E.B., 2003. The presence of the casein kinase II phosphorylation sites of Vpu enhances the $CD4^+$ T cell loss caused by the simian-human immunodeficiency virus SHIV$_{KU\text{-}1bMC33}$ in pig-tailed macaques. Virology 313, 435–451.

Stephens, E.B., Sahni, M., Leung, K., Raghavan, R., Joag, S.V., Narayan, O., 1998. Nucleotide substitutions in the long terminal repeat are not required for development of neurovirulence by simian immunodeficiency virus strain mac. J. Gen. Virol. 79, 1089–1100.

Stephens, E.B., McCormick, C., Pacyniak, E., Griffin, D., Pinson, D.M., Sun, F., Nothnick, W., Wong, S.W., Gunderson, R., Berman, N.E., Singh, D.K., 2002. Deletion of the vpu sequences prior to the env in a simian-human immunodeficiency virus results in enhanced Env precursor synthesis but is less pathogenic for pig-tailed macaques. Virology 293, 252–261.

Teo, I., Veryard, C., Barnes, H., An, S.F., Jones, M., Lantos, P.L., Luthert, P., Shaunak, S., 1997. Circular forms of unintegrated human immunodeficiency virus type 1 DNA and high levels of viral protein expression: association with dementia and multinucleated giant cells in the brains of patients with AIDS. J. Virol. 71, 2928–2933.

Tiganos, E., Friborg, J., Allain, B., Daniel, N.G., Yao, X.J., Cohen, E.A., 1998. Structural and functional analysis of the membrane-spanning domain of the human immunodeficiency virus type 1 Vpu protein. Virology 251, 96–107.

Varthakavi, V., Smith, R.M., Bour, S.P., Strebel, K., Spearman, P., 2003. Viral protein U counteracts a human host cell restriction that inhibits HIV-1 particle production. Proc. Natl. Acad. Sci. U.S.A. 100, 15154–15159.

Zazzi, M., Romano, L., Catucci, M., Venturi, G., De Milito, A., Almi, P., Gonnelli, A., Rubino, M., Occhini, U., Valensin, P.E., 1997. Evaluation of the presence of 2-LTR HIV-1 unintegrated DNA as a simple molecular predictor of disease progression. J. Med. Virol. 52, 20–25.